Nanoscale

Assembling Si2BN nanoribbons to a 3D porous structure as a universal anode material for both Li- and Na-ion batteries with high performance

Journal:	*Nanoscale*
Manuscript ID	NR-ART-07-2020-005143.R1
Article Type:	Paper
Date Submitted by the Author:	17-Aug-2020
Complete List of Authors:	Younis, Umer; Peking University, Material science and engineering ; Peking University, Material science and engineering Imran, Muhammad; Peking University, Department of Materials Science and Engineering College of Engineering Wu, Wei; Peking University, ahmed, Shehzad; Xi'an Jiaotong University Sun, Qiang; Peking University, Jena, Purusottam ; Virginia Commonwealth University, Physics Department

Assembling Si_2BN nanoribbons to a 3D porous structure as a universal anode material for both Li- and Na-ion batteries with high performance

Umer Younis [a], Imran Muhammad [a], Wei Wu [a], S. Ahmed [b], Qiang Sun [a,c,*], Puru Jena[d]

[a] Department of Materials Science and Engineering, Peking University, Beijing 100871, China.

[b] Center for Advancing Materials Performance from the Nanoscale, State Key Labortory for Mechanical Behavior of Materials, Xi'an Jiaotong University, Xi'an 710049 China.

[c] Center for Applied Physics and Technology, Peking University, Beijing 100871, China.

[d] Department of Physics, Virginia Commonwealth University, Richmond, VA 23284, USA.

ABSTRACT

Development of anode materials is critical to the success of sodium ion batteries (SIBs). Because of the size difference between Li and Na, the commercial anode material graphite in Li-ion battery does not work for Na-ion battery. Thus, it will be ideal if some universal anode materials could work for both Li- and Na-ion batteries with high performance. Inspired by the recent study on the high performance of 2D-Si_2BN sheet as an anode material of Li-ion battery, we design a three dimensional (3D) porous structure by using the nanoribbons of Si_2BN sheet as the building blocks. Based on state-of-the-art *ab initio* calculations, we find that the resulting 3D porous Si_2BN structure is stable chemically, dynamically and thermally, exhibiting high specific capacity of 512.42 (341.61 mAh/g), low voltage of 0.27 V (0.15 V), small volume expansion of 2.5% (2.7%), and low migration energy barrier of 0.44 eV (0.19 eV) for Li- (Na-) ion batteries. These intriguing features, together with the light mass and rich abundance of Si, B and N, suggest that the 3D porous Si_2BN is a promising candidate for the anode material of both Li- and Na-ion batteries.

1. INTRODUCTION

Energy storage systems have great technological importance because of their applications in electric vehicles, electronic devices, and power grid systems.[1,2] Among different energy storage systems, Li-ion batteries (LIBs) and Na-ion batteries (NIBs) have been hotly studied.[3–7] However, LIBs suffer from cost issues, safety, and limited specific capacity,[8] while NIBs are plagued by significant volume expansion, poor capacity retention, and anode degradation.[9] In addition, due to

the large difference in size between Li- and Na-ion, only a few electrode materials such as SnO_2/C,[10] 3D honeycomb-like SnS_2,[11] SnS/C nanocomposites,[12] exhibit optimal electrochemical properties for both Li and Na-ion.[13] Therefore, design of new electrode materials that work for multiple ions with high performance is of significance both scientifically and technogically. In recent years, Si-based two-dimensional (2D) and three-dimensional (3D) porous materials have been explored for different applications,[14,15] specially for batteries which have attracted intensive attention due to its light mass, high theoretical capacity (4200 mAh/g for LIB) and low discharge potential.[16] Although this capacity is several times higher than that of commercially available graphite, nitride and oxide materials,[17,18] the applicability of silicon anode is constrained by the huge volumetric change of >300 % during charging and discharging. This results in weak stability and capacity fading.[19] In order to overcome such problems, other elements are introduced to Si for stabilization such as Si-Ge,[20] Si_2BN,[21] Si@void@C,[22] porous SiC_4 allotropes,[23] Si/C spheres,[24] C_2Si,[25] and doped Si-nanowires.[26] Recently, a stable Si_2BN sheet has been proposed as an anode material for Li and Na-ion batteries that exhibit intriguing properties such as high charge mobility, tunable energy band, and high-performance.[27] For practical applications, however, a 3D porous material is highly desirable as compared with a single 2D sheet. Actually, one of current frontiers in materials research is to assemble 2D sheets for 3D functional materials, and many 3D graphene-based porous structures have been successfully synthesized [28–32].

However, Si-based 3D porous materials with desired properties are much less explored. This raises an interesting question: can we find a 3D porous Si_2BN structure with high performance that is stable as anode material for both LIBs and NIBs? In this work, for the first time, we propose a porous 3D-Si_2BN by assembling the nanoribbons of 2D monolayer Si_2BN, which is found to be meta-stable energetically while stable chemically, dynamically and thermally, displaying high theoretical capacity and low energy barriers for both Li and Na ions.

2. COMPUTATIONAL DETAIL

All calculations are based on density functional theory as implemented in the Vienna *Ab-initio* Simulation Package.[33] For electron-electron exchange-correlation and electron-ion interaction, we use Perdew-Burke-Ernzerhof functional (PBE) and projector augmented wave (PAW) methods with a cutoff energy of 520 eV and (4×4×8) k-mesh.[34,25] For electronic band structure calculations, the hybrid Hyed-Seuseria-Ernzerhof (HSE06) functional is also employed.[35] Structure

optimization is carried out using the conjugate gradient method with convergence criteria of 10^{-6} eV for energy and 10^{-3} eV/Å for the force. The van der Waals interaction is included through long-range dispersion correction by the Grimme PBE-D3 method. The charge population analysis and migration barrier are computed by using Bader charge and climbing-image nudged elastic band (CI-NEB) techniques, respectively.[36,37] The structural stability is confirmed by calculating the phonon spectrum within the framework of finite displacement method as implemented in phonopy code.[38] Furthermore, *ab initio* molecular dynamics (AIMD) simulation[39] is also used to check the thermal stability at 600K.

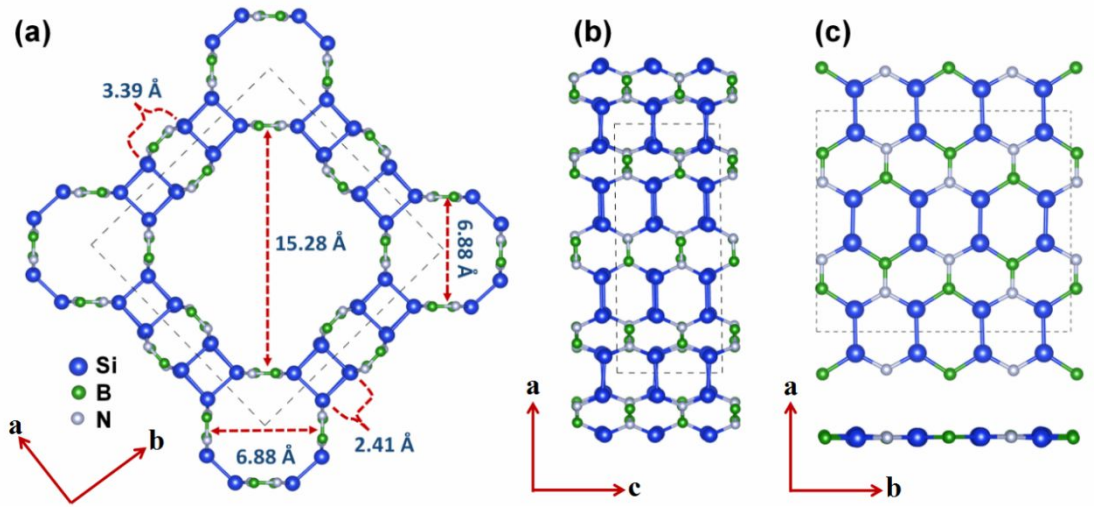

Figure. 1 Unit cell in different views (a-b) of porous 3D-Si_2BN, and the geometry of 2D-Si_2BN sheet (c) is also given for comparison.

3. RESULTS AND DISCUSSION

3.1 Geometry

A porous 3D Si_2BN structure is constructed by using nanoribbons of 2D-Si_2BN as building blocks, the resulting geometry is isostructural to tC_{24} [40] when substituting C with Si, B and N. The unit cell contains 64 atoms with a space group *Cccm* (no. 66). The fully relaxed lattice parameters of the structure are $a = b = 15.37$ Å and $c = 6.43$ Å, with the Si atoms occupying three positions as shown in **Fig. 1.** The bond lengths in the optimized geometry are found to be Si-Si = 2.39 Å, Si-B = 2.0 Å, Si-N = 1.79 Å and B-N = 1.41 Å. The corresponding bond angles are Si-B-Si =

111.76°, Si-N-Si = 116.33°, B-Si-N = 116.91°, Si- Si-B = 111.09°, Si-Si-N = 115.79° and N-B-Si = 118.63°. In addition, this porous 3D structure exhibits four different channels along the *c*-direction with a pore size of 15.28, 6.88, 3.39 and 2.41 Å, respectively. The corresponding mass density is 1.41 g cm^{-3}, which is less than the values of other anode materials, as shown in **Table 1.**

Table. 1 Comparison of space group, and density of 3D-Si_2BN with some previously reported systems.

System	Group	ρ (g/cm^3)
3D-Si_2BN	*Cccm*	1.41
SiC_4 allotrope (SiC_4-I)[23]	*Pmmm*	2.20
Graphite[41]	*$P6_3/mmc$*	2.24
Silicene-based 3D network [42]	*Cmcm*	1.63
Silicon allotrope (Si-I)[43]	*Fd-3m*	2.38
Porous Si_{24}[44]	*Cmcm*	2.17

3.2 Stability

To investigate the stability, we calculate the phonon band structure of 3D-Si_2BN by using the phonopy code. The phonon spectrum in **Fig. 2(a)** clearly shows no imaginary mode in the whole Brillion zone, confirming the dynamical stability of the structure, although the energy of 3D-Si_2BN is above the hull as shown in **Fig. S1** in supporting information (**SI**), it is energetically meta-stable. We then check the thermal stability at 300 and 600 K using *ab initio* molecular dynamics (AIMD) simulation for 10ps with a time step of 1fs. The results are given in **Fig. 2(b)**, confirming thermal stability of porous 3D-Si_2BN. Furthermore, to check the chemical bonding stability, we use crystal orbital Hamilton population (COHP) analysis that partitions the band-structure energy into orbital-pair interactions, where bonding is characterized by a positive overlap population and the corresponding Hamiltonian off-site element will then be negative, while the antibonding interactions exhibit positive off-site Hamiltonian elements. COHP can intuitively and clearly exhibit the contributions of pairs of atoms to the structural stability of materials: the negative COHP gives the bonding contribution below the Fermi level, whereas the positive COHP gives the antibonding contribution. The calculated COHP is added in Fig.1(c), where there is no

occupied antibonding state at the Fermi level, clearly showing the chemical bonding stability of 3D-Si2BN. Moreover, the strength of different chemical bonds in 3D-Si_2BN is also investigated by employing projected COHP, among the bonding pairs of N-B, N-Si, B-Si, and Si-S, the last two are the stronger than the first two.

In addition, the energetic stability is studied by calculating the average energy per atom *(E)* of the system and using the following relation: [45]

$$E = -(E_{total} - n_{Si}E_{Si} - n_BE_B - n_NE_N)/M \quad (1)$$

where E_{total}, E_{Si}, E_B, and, E_N are the total energy of porous 3D-Si_2BN, the energy of Si, B, and N atoms in free state, respectively. n_{Si}, n_B, and n_N are the number of Si, B and N atoms in porous 3D-Si_2BN, and $M = n_{Si} + n_B + n_N$. The value of E is 6.56 eV, suggesting that 3D-Si_2BN is energetically more stable than diamond SiC_4 (6.48 eV)[23] and iron silicides series (6.30 eV).[46] Moreover, we have also constructed two other structures of 3D porous Si_2BN, which are shown in **Fig. S2(a, b)** in SI. Both are found to be less stable compared to the one shown in **Fig. 1**.

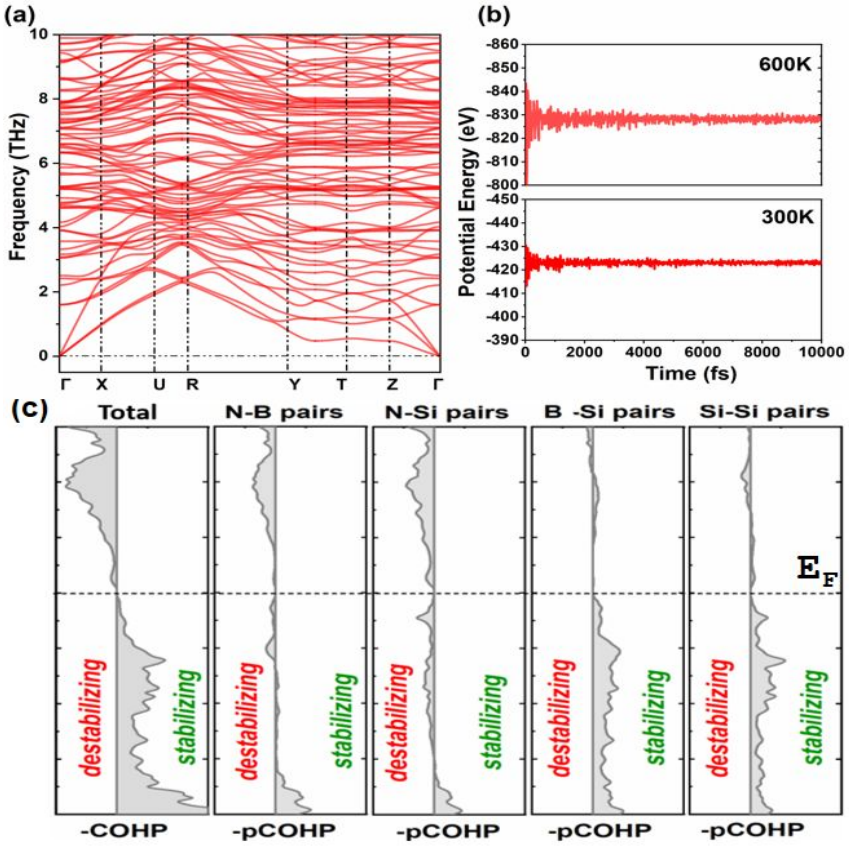

Figure. 2 (a) Phonon spectrum of porous 3D-Si_2BN (b) Fluctuation of potential energy at 300 and 600 K during AIMD. (c) The total and projected crystal orbital Hamilton population (COHP) for 3D-Si_2BN.

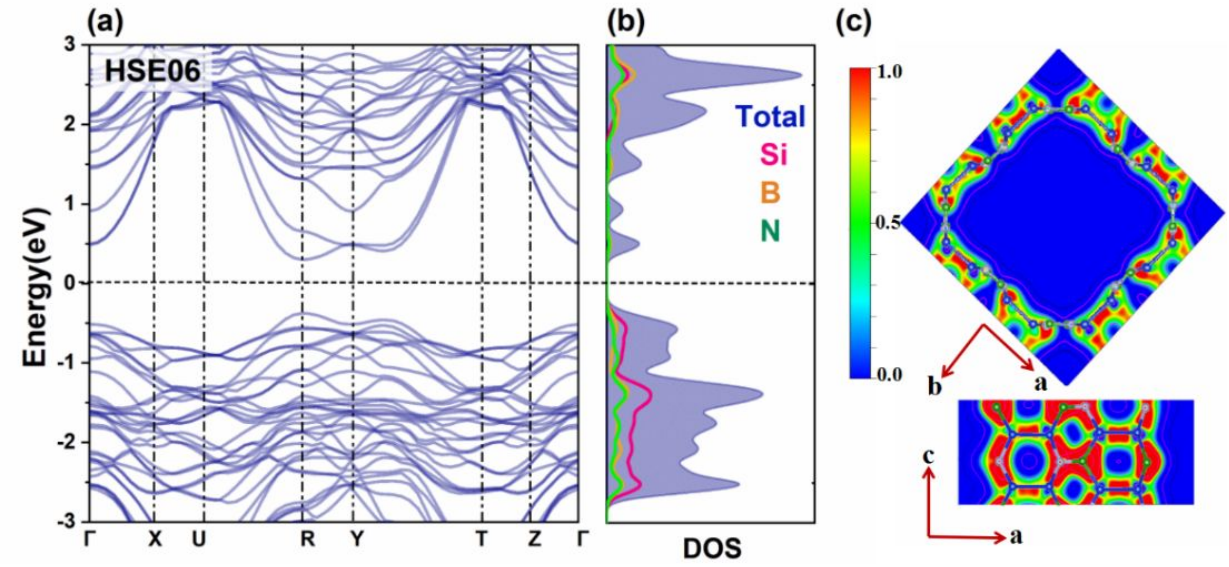

Figure.3 (a-b) Electronic band structure and partial density of states calculated using HSE-06 functional. (c) The ELF slices parallel to ***ab***, and ***ac*** plane of 3D-Si_2BN.

3.3 Electronic Properties

In order to understand the electronic structure and chemical bonding of 3D porous Si_2BN, we calculate the electron localization function (ELF) with values renormalized in the range of 0.0 and 1.0, which correspond to the region of low-density and fully localized electron, respectively. The region with 0.5 represents full delocalization of electrons. The ELF slices parallel to ***ab,*** and ***ac*** planes are shown in **Fig. 3(c),** indicating strong covalent bonding formed between Si, B and N atoms. Moreover, due to the difference in electronegativity between Si and B/N, charges transfer from Si to N and B, resulting in polarized bonding. Next, we calculate the electronic band structure. Unlike metallic 2D-Si_2BN[27], the 3D system is a semiconductor with a narrow direct band gap of 0.67 eV calculated using the HSE06 functional as shown in **Fig. 3(a)** and **3(b)** for band and density of states (DOS).

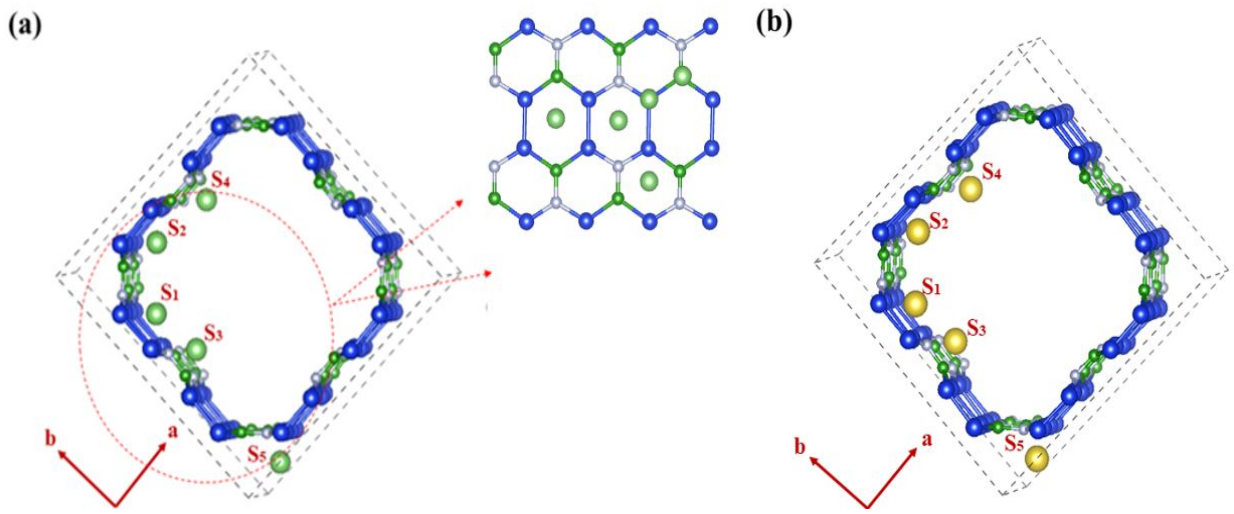

Figure. 4 Electrochemically active sites for Li (a) and Na (b).

3.4 Application as anode material for Li and Na-ion batteries

The regularly distributed channels in porous 3D-Si_2BN structure suggest their potential as a anode material for LIBs and NIBs. To check this point, we investigate the adsorption strength of single Li/Na atom on the 3D-Si_2BN substrate by using the following equation:[47]

$$E_b = (E_{Li/Na+(3D\text{-}Si2BN)} - E_{3D\text{-}Si2BN} - E_{Li/Na}) \quad (2)$$

where $E_{Li/Na+(3D\text{-}Si2BN)}$ and $E_{3D\text{-}Si2BN}$ are the energies of Li/Na-inserted and pristine 3D-Si_2BN structure, respectively, and $E_{Li/Na}$ is the chemical potential of bulk Li/Na metal (energy per metal atom in the bulk metal). Based on the geometrical symmetry, we initially consider five adsorption sites for both Li and Na ions, including the three hollow sites (S_1, S_2, S_3) of Si_4N_2, Si_4B_2, and $Si_2B_2N_2$ rings, one top site (S_4) of B and one top site (S_5) on Si in $Si_2B_2N_2$ ring, as shown in **Fig. 4 (a, b).** The corresponding adsorption energies are -0.85, -0.79, -0.75, -0.73, and -0.45 eV for Li, and -0.84, -0.80, -0.77, -0.82, -0.69 eV for Na, respectively. In order to understand the interaction of Li/Na ions with 3D substrate at these sites, we calculate the partial density of states (PDOS) as plotted in **Figs. S3** and **S4** of SI.

To study the charge transfer on each site, we use Bader charge analysis. The corresponding calculated values are 0.88, 0.86, 0.88, 0.87, 0.88 *e* for Li, and 0.86, 0.87, 0.84, 0.87, 0.86 e for Na, respectively. The significant charge transfer not only leads to strong adsorption, but also large van

der Waals interaction due to strong polarization induced by the charge transfer. The results are summarized in **Table 2**. Information on charge transfer can also be seen from charge density difference $\Delta\rho$ defined as $\Delta\rho = \rho_{3D\text{-}Si2BN+Li/Na} - \rho_{3D\text{-}Si2BN} - \rho_{Li/Na}$. The results are given in **Fig. 5 (a, b)**, where red and blue colors are for charge loss and charge gain, respectively. Additionally, we also calculate the charge density difference at the second most stable sites (Si_4B_2) which is presented in **Fig.S5.**

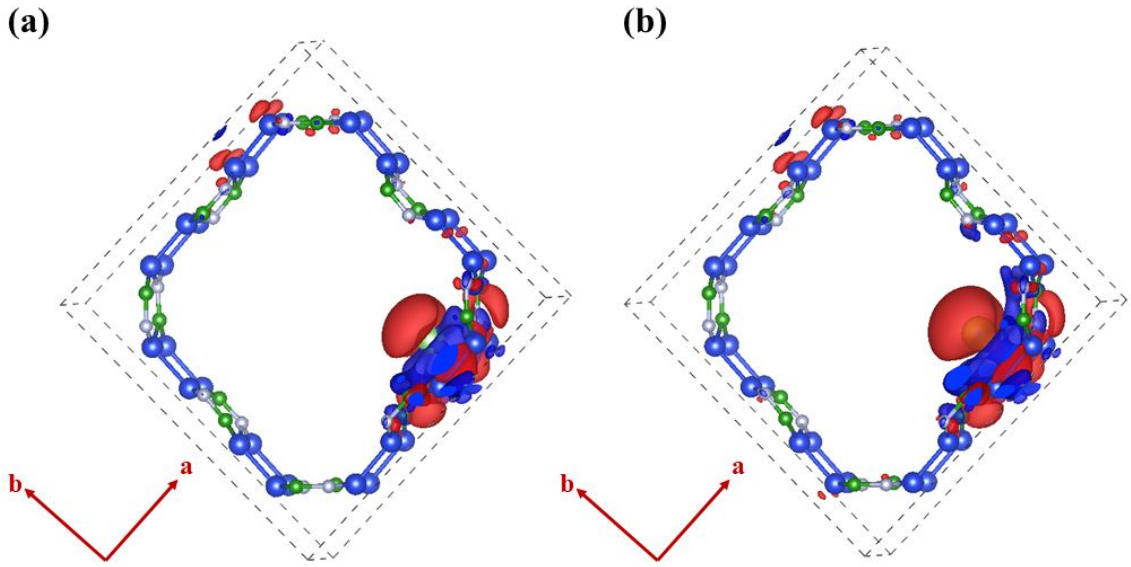

Figure. 5 Charge density difference for (a) lithium and (b) sodium-ions at the most stable site (Si_4N_2) in 3D-Si_2BN.

Next, we calculate the migration barrier associated with Li and Na ion diffusion. According to the geometrical symmetry of 3D-Si_2BN, we take two typical migration pathways for hollow site diffusion as plotted in **Fig. 6(b):** path-I: $S_2 \rightarrow S_1 \rightarrow S_2$, and path-II: $S_2 \rightarrow S_3 \rightarrow S_2$. Using nudged elastic band (NEB) calculations, the energy barriers for Li ion along these two paths are found to be 0.47 and 0.44 eV, respectively, whereas for Na-ion the corresponding values are 0.19 and 0.21 eV. These are smaller than the barrier in bulk silicon[48] and Si_{24}.[8] Moreover, the barrier for Na-ion diffusion is smaller than that for Li-ion along the same path due to the larger size of Na and the weaker interaction energy of Na with the surface because of the weaker charge-surface interactions.

To check the capacity and the stability, we consider six (four) different concentrations for lithium (sodium) ions, which are presented in **Figs. S6** and **S7** of **SI**. We further perform molecular dynamics simulation at room temperature (300 K) for 5 ps with time step of 1 fs. It turns out that

all the considered configurations are stable (see **Figs. S8 and S9**). In addition, the formation energy of convex hull is also calculated at the various concentrations of sodium ions which is presented in **Fig. S10** of the SI and make sure the stability of intermediate phases.

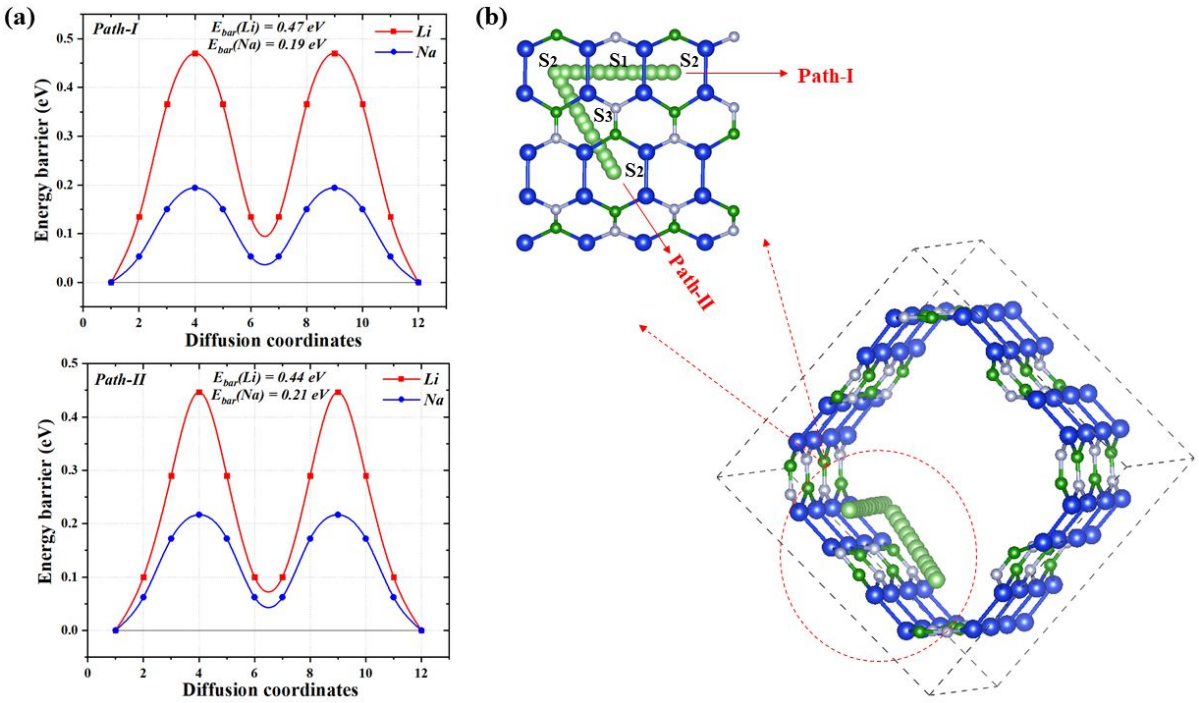

Figure. 6 (a) Energy barrier profile for Li/Na diffusion. (b) Two pathways.

Table.2 Binding energy E_b(in eV) with and without van der Waals interaction correction and charge transfer Q (in *e*) of Li and Na ions on different sites in 3D-porous Si_2BN.

Binding Sites	**E_b of Li**		**E_b of Na**		**Q (Li)**	**Q (Na)**
	VdW	*no VdW*	*VdW*	*no VdW*		
S_1 (Si_4N_2)	-0.85	-0.68	-0.84	-0.68	0.88	0.86
S_2 (Si_4B_2)	-0.79	-0.67	-0.80	-0.63	0.86	0.84
S_3 ($Si_2B_2N_2$)	-0.75	-0.30	-0.77	-0.12	0.88	0.87
S_4 (B-Top)	-0.73	-0.57	-0.82	-0.58	0.87	0.87
S_5 (Si-Top)	-0.45	-0.34	-0.69	-0.48	0.88	0.86

The maximum capacity *C* for Li- and Na-ion in 3D-Si_2BN can be found by using the following relationship:[27]

$$C = xF/3.6M_{3D\text{-}Si2BN} \quad (3)$$

where *x* represents the numbers of metal ions that are adsorbed on Si_2BN substrate, F is Faraday's constant (96,485.3329 s A mol^{-1}), and M is the molar mass of 3D-Si_2BN. The maximum theoretical capacity calculated for Li (Na) ions is 512.42 mAh/g (341.61 mAh/g). which is, respectively, higher than the value for Li in graphite (372 mAh/g) and the value for Na in topological nodal-line semimetal porous Si (159.5 mAh/g).

To check the mechanical stability of 3D-Si_2BN during operation, the volume change is calculated during charging and discharging, which is found to be 2.5% and 2.7% for Li and Na ions. These values are much less than those of values of Li in graphite (10.3%) and Na in amorphous Si (227%).

Another key quantity for measuring the efficiency of a battery is the average voltage V defined as: [49]

$$V = -[E_{Mx(3D\text{-}Si2BN)} - E_{3D\text{-}Si2BN} - xE_{M(bulk)}]/Zxe \quad (4)$$

where $E_{Mx(3D\text{-}Si2BN)}$ and $E_{3D\text{-}Si2BN}$ are the energy of the system with or without metal ions, $E_{M(bulk)}$ is energy of metal ion in the bulk structure, and *x* is the number of metal ions. As shown in **Fig.7(b)**, the average voltage for the Li and Na ion is 0.27 V and 0.15 V respectively, which is comparable to the value of graphite (~0.11V) and is within the desired voltage window of 0.1~1.0 V [50].

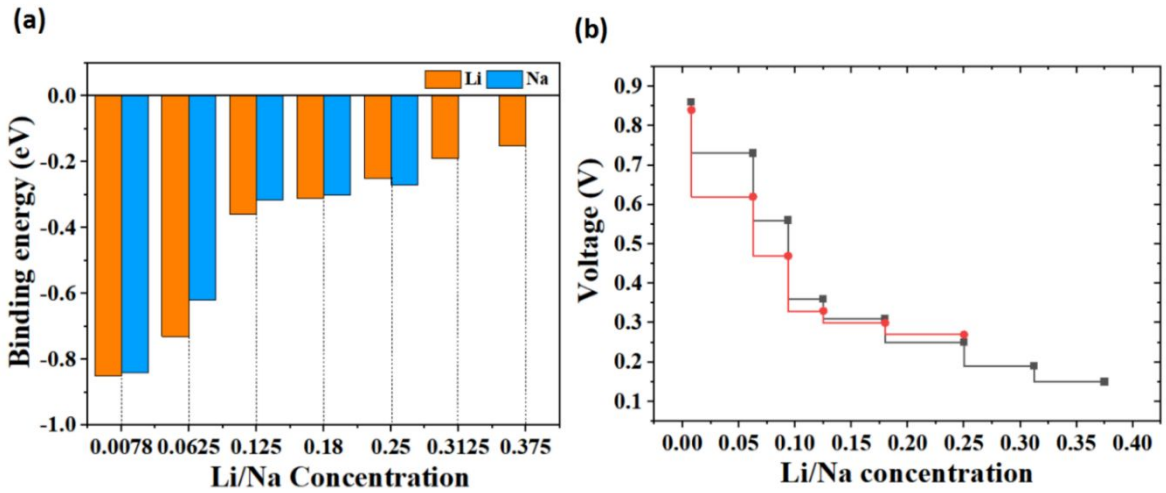

Figure. 7 (a) Binding energies of Li- and Na-ion with substrate changing with concentrations; (b) Average voltage changing with ion concentration in the range of 0.078-0.375

In order to compare the *overall* performance of 3D-Si_2BN with some other Si-based materials (graphite is also included for comparison), we summarize the values of the migration barrier, specific capacity, volume change, voltage, as well as the electronic band in **Table. 3**. One can clearly see that the potential of 3D-Si_2BN is very promising for Li-ion as well as for Na-ion, namely, it is a universal anode material for these two batteries.

Table. 3 Comparison of specific capacity, migration barrier, volume change, voltage (V), and the electronic band of Si-based anode materials for Li and Na-ion batteries. ('—' means data unavailable)

Materials	**Capacity (mAh/g)**		**Migration barrier (eV)**		**Volume change (%)**		**Voltage (V)**		**Electronic Band**
	(Li)	**(Na)**	**(Li)**	**(Na)**	**(Li)**	**(Na)**	**(Li)**	**(Na)**	
3D-Si_2BN	512.42	341.61	0.44	0.19	2.5	2.7	0.27	0.15	Semiconducting
2D-Si_2BN[27]	1158.5	993.0	0.48	0.32	_	_	0.46	0.27	Metallic
Graphite[51]	372	_	0.21-0.4	_	10	_	0.11	_	Metallic
Sillicon[16,25,48,52]	4200	_	0.58	_	>300	_	0.28	_	Semiconducting
Silicene-based 3D network[42]	_	159.5	_	0.005	2.80	_	_	1.35	Topological nodal-line semimetallic
Si_{24}[8]	_	159.5	_	0.68	_	2.30	_	0.30	Metallic
T-C_2Si[25]	515		0.26-0.78	_	1.6	_	1.14	_	Metallic
SiC4-I[23]	_	176.3	_	0.41	_	0.57		0.55	Metallic
Silicene[53]	_	954	_	0.16	_	_		0.3-0.5	Dirac semimetallic
Amorphous-Si[9]		957		0.31		227		_	Semiconducting

4. Summary

Based on first-principles calculations we propose a stable 3D porous Si_2BN structure, which consists of Si_2BN nanoribbons as repeating building blocks. The 3D-Si_2BN has three different in-plane hexagonal rings and four different pores along the c-direction. This porous configuration is highly stable and exhibits a direct semiconducting character with a narrow band gap of 0.67 eV. As a "universal anode material" for both LIB and NIB, the 3D-Si_2BN displays the following charactersitics: (1) high theoretical capacities of 512.41 and 341.61 mAh/g; (2) low migration barriers of 0.44 and 0.19 eV; (3) low average voltages of 0.27 and 0.15 V, (4) small volume changes of 2.5% and 2.7 % for Li and Na ions, respectively. This study not only expands the Si-B-N based structures from 2D to 3D but also sheds light on the design of novel porous materials for high-performance battery applications.

ACKNOWLEDGMENTS

This work was partially supported by grants from the National Natural Science Foundation of China (21973001), and from the National Key Research and Development Program of China (2016YFB0100200). P. J. acknowledges partial support by the U.S. Department of Energy, Office of Basic Energy Sciences, Division of Materials Sciences and Engineering under Award DE-FG02-96ER45579. The calculations were supported by High-performance Computing Platform of Peking University.

References

1 D. Er, J. Li, M. Naguib, Y. Gogotsi and V. B. Shenoy, *ACS Appl. Mater. Interfaces*, 2014, **6**, 11173–11179.

2 I. Muhammad, U. Younis, H. Xie, Y. Kawazoe and Q. Sun, *Adv. Theory Simulations*, 2020, **1900236**, 1900236.

3 R. Jana, C. Chowdhury and A. Datta, *ChemSusChem*, (2020).

4 H. Xie, Y. Qie, M. Imran and Q. Sun, *J. Mater. Chem. A*, 2019, **7**, 14253–14259.

5 B. Scrosati and J. Garche, *J. Power Sources*, 2010, **195**, 2419–2430.

6 A. Bai, L. Wang, J. Li, X. He, J. Wang and J. Wang, *J. Power Sources*, 2015, **289**, 100–104.

7 S. Karmakar, C. Chowdhury and A. Datta, *J. Phys. Chem. C*, 2016, **120**, 14522–14530.

8 U. Arrieta, N. A. Katcho, O. Arcelus and J. Carrasco, *Sci. Rep.*, 2017, **7**, 1–8.

9 C. Y. Chou, M. Lee and G. S. Hwang, *J. Phys. Chem. C*, 2015, **119**, 14843–14850.

10 J. I. Lee, J. Song, Y. Cha, S. Fu, C. Zhu, X. Li, Y. Lin and M. K. Song, *Nano Res.*, 2017, **10**, 4398–4414.

11 Y. Zhang, Y. Guo, Y. Wang, T. Peng, Y. Lu, R. Luo, Y. Wang, X. Liu, J. K. Kim and Y. Luo, *Nanoscale Res. Lett.*, 3 (2008): 201

12 C. Zhu, P. Kopold, W. Li, P. A. van Aken, J. Maier and Y. Yu, *Adv. Sci.*, 2015, **2**, 1–8.

13 C. Chowdhury, S. Karmakar and A. Datta, *ACS Energy Lett.*, 2016, **1**, 253–259.

14 D. Jose and A. Datta, *Acc. Chem. Res.*, 2014, **47**, 593–602.

15 S. M. Pratik, A. Nijamudheen and A. Datta, *Chem. - A Eur. J.*, 2015, **21**, 18454–18460.

16 C. K. Chan, H. Peng, G. Liu, K. McIlwrath, X. F. Zhang, R. A. Huggins and Y. Cui, *Nat. Nanotechnol.*, 2008, **3**, 31–35.

17 T. Shodai, S. Okada, S. I. Tobishima and J. I. Yamaki, *Solid State Ionics*, 1996, **86**–**88**, 785–789.

18 P. Poizot, S. Laruelle, S. Grugeon, L. Dupont and J. Tarascon, (2000), 407(6803), 496-499.

19 L. Y. Beaulieu, K. W. Eberman, R. L. Turner, L. J. Krause and J. R. Dahna, *Electrochem. Solid-State Lett.*, 2001, **4**, 10–13.

20 A. Sannyal, Y. Ahn and J. Jang, *Comput. Mater. Sci.*, 2019, **165**, 121–128.

21 D. Singh, S. K. Gupta, Y. Sonvane, T. Hussain and R. Ahuja, *Phys. Chem. Chem. Phys.*, 2018, **20**, 21716–21723.

22 F. Wang, B. Wang, T. Ruan, T. Gao, R. Song, F. Jin, Y. Zhou, D. Wang, H. Liu and S. Dou, *ACS Nano*, 2019, **13**, 12219–12229.

23 Y. Qie, S. Wang and Q. Sun, *Nano Energy*, 2019, **63**, 1–7.

24 G. Hou, B. Cheng, Y. Cao, M. Yao, B. Li, C. Zhang, Q. Weng, X. Wang, Y. Bando, D. Golberg and F. Yuan, *Nano Energy*, 2016, **24**, 111–120.

25 J. Liu, S. Wang, Y. Qie, J. Yu and Q. Sun, *Carbon N. Y.*, 2018, **140**, 680–687.

26 M. Ge, J. Rong, X. Fang and C. Zhou, *Nano Lett.*, 2012, **12**, 2318–2323.

27 V. Shukla, R. B. Araujo, N. K. Jena and R. Ahuja, *Nano Energy*, 2017, **41**, 251–260.

28 Z. Fang, Q. Xing, D. Fernandez, X. Zhang and G. Yu, *Nano Res.*, (2010) 13(5), 1179-1190.

29 K. Chen, L. Shi, Y. Zhang and Z. Liu, *Chem. Soc. Rev.*, 2018, **47**, 3018–3036.

30 K. Kim, T. Lee, Y. Kwon, Y. Seo, J. Song, J. K. Park, H. Lee, J. Y. Park, H. Ihee, S. J. Cho and R. Ryoo, *Nature*, 2016, **535**, 131–135.

31 N. V. Krainyukova and E. N. Zubarev, *Phys. Rev. Lett.*, 2016, **116**, 1–5.

32 M. Zhang, K. Chen, C. Wang, M. Jian, Z. Yin, Z. Liu, G. Hong, Z. Liu and Y. Zhang, *Small*, 2018, **14**, 1–9.

33 F. Wende, M. Marsman, J. Kim, F. Vasilev, Z. Zhao and T. Steinke, *Int. J. Quantum Chem.*, 2019, **119**, 1–17.

34 H. Cu and H. Ag, (2019), 123(25), 5395-5406.

35 J. C. Phys, P. G. Moses, M. Miao, Q. Yan and C. G. Van De Walle, (2011), 134(8), 084703.

36 G. Henkelman, B. P. Uberuaga and H. Jónsson, *J. Chem. Phys.*, 2000, **113**, 9901–9904.

37 G. Henkelman and H. Jónsson, *J. Chem. Phys.*, 2000, **113**, 9978–9985.

38 A. Togo and I. Tanaka, *Scr. Mater.*, 2015, **108**, 1–5.

39 U. Younis, I. Muhammad, Y. Kawazoe and Q. Sun, *ChemPhysChem*, (2019), 20(21), 2799-2805.

40 Y. Qie, J. Liu, S. Wang, Q. Sun and P. Jena, *J. Mater. Chem. A*, 2019, **7**, 5733–5739.

41 Z. Zhao, B. Xu, L. M. Wang, X. F. Zhou, J. He, Z. Liu, H. T. Wang and Y. Tian, *ACS Nano*, 2011, **5**, 7226–7234.

42 Y. Qie, J. Liu, X. Li, S. Wang, Q. Sun and P. Jena, *Phys. Rev. Mater.*, 2018, **2**, 1–7.

43 Q. Wang, B. Xu, J. Sun, H. Liu, Z. Zhao, D. Yu, C. Fan and J. He, *J. Am. Chem. Soc.*, 2014, **136**, 9826–9829.

44 D. Y. Kim, S. Stefanoski, O. O. Kurakevych and T. A. Strobel, *Nat. Mater.*, 2015, **14**, 169–173.

45 R. B. Dos Santos, R. Rivelino, F. De B. Mota and G. K. Gueorguiev, *J. Phys. Chem. A*, 2012, **116**, 9080–9087.

46 R. Podloucky, *Phys. Rev. B - Condens. Matter Mater. Phys.*, 1999, **59**, 12860–12871.

47 U. Younis, I. Muhammad, Y. Kawazoe and Q. Sun, *Appl. Surf. Sci.*, (2020), 146456.

48 W. Wan, Q. Zhang, Y. Cui and E. Wang, *J. Phys. Condens. Matter*, (2010), 22(41), 415501.

49 A. Samad, A. Shafique and Y. H. Shin, *Nanotechnology*, (2017), 28(17), 175401.

50 K. Persson, Y. Hinuma, Y. S. Meng, A. Van Der Ven and G. Ceder, *Phys. Rev. B - Condens. Matter Mater. Phys.*, 2010, **82**, 1–9.

51 M. Armand, *Nature*, 2001, **414**, 359–367.

52 T. Journal, M. C. Weeks, T. Journal, M. C. Weeks, E. Voss, S. Yoshizawa, S. Okada, R. T. Mathieson, P. Press, E. L. Jones, T. Journal, G. Papazov, D. Pavlov, T. M. Company, E. J. Ritchie and C. Manufacturing, (1981), 128(4), 725.

53 J. Zhu and U. Schwingenschlögl, *2D Mater.*, (2016), 3(3), 035012.